Geotech Geol Eng (2019) 37:3241–3253
https://doi.org/10.1007/s10706-019-00839-8

ORIGINAL PAPER

Effect of Curing Temperature on Mechanical Performance and Acoustic Emission Properties of Cemented Coal Gangue-Fly Ash Backfill

Di Wu · Runkang Zhao · Chunlai Qu

Received: 5 March 2018 / Accepted: 19 February 2019 / Published online: 25 February 2019

Abstract Cemented coal gangue-fly ash backfill (CGFB), which is a mixture of coal gangue, fly ash, binder and water, is introduced and employed to fill underground mined-out areas of coal mines. Once placed, the CGFB mixtures should have favorable stability, which is closely relevant to the mechanical performance of the CGFBs. The mechanical behavior of CGFB is affected by the environment temperature. In this study, with the help of acoustic emission (AE) and infrared thermal imaging technique, the influence of curing temperature on the mechanical behavior of CGFB specimens is investigated. A uniaxial compressive strength (UCS) testing apparatus coupled with AE monitoring and infrared thermography is equipped to investigate the mechanical (UCS, elastic modulus, stress–strain relation), acoustic (AE cumulative counts and energy), and thermal (average infrared radiation temperature) properties of CGFB samples cured for different ages (1, 3 and 7 days) at various curing temperatures (20, 50, 75 and 90 °C). This study provides an effective coupled monitoring method for evaluating the performance of CGFB structures, and this can contribute to a better understanding of the thermo-mechanical-acoustic behavior of CGFBs, and thus a better design of stable CGFBs.

Keywords Cemented coal gangue-fly ash backfill · Mechanical performance · Acoustic emission · Curing temperature · Infrared thermography

1 Introduction

In recent years, cemented coal gangue-fly ash backfill (CGFB), which is a mixture of binder, coal gangue, fly ash and water, is utilized to fill mined-out areas of underground coal mines in China for both ground control and waste management (Wu et al. 2015a, b, 2016a, b, 2017). Since the CGFB is placed to support the roof (Wu et al. 2015a, b), it should possess sufficient stability. Consequently, mechanical performance has to be one of the most significant criteria for evaluating the CGFB structure. In practice, the uniaxial compressive strength (UCS) test is often used to indicate and assess the mechanical stability of CGFB. The UCS values of CGFBs are largely affected by both the own conditions of the CGFB materials

D. Wu (✉) · R. Zhao
School of Energy and Mining Engineering, China University of Mining and Technology-Beijing, Beijing, People's Republic of China
e-mail: ustb_wudi@hotmail.com

D. Wu
School of Civil, Environmental and Mining Engineering, The University of Western Australia, Perth, Australia

C. Qu
College of Water Conservancy and Hydropower, Hebei University of Engineering, Handan, People's Republic of China

(such as the physical and chemical properties of the ingredients, water to binder ratio, binder content and so on) and the external factors (e.g., ambient temperature). For a cemented material such as CGFB, the curing temperature, which mainly affects the progress of binder hydration, exerts a significant effect on the UCS. However, no studies have investigated the effect of curing temperature on the UCS of CGFB.

For other kinds of cement-based materials such as concrete and CPB (cemented paste backfill, a mixture of tailings and hydraulic binder), the influence of curing temperature on their mechanical performance has been studied and reported. For instance, Zhao et al. (2015) have investigated the creep behavior of various fly ash concretes under the curing temperatures of 20 °C, 50 °C and 90 °C. Orosz et al. (2017) have examined the effects of variable curing temperatures (6, 35 and 50 °C) on autogenous deformation of blended cement concretes. Xu et al. (2017) have analyzed the mechanical properties of slag and fly ash concretes at different curing temperatures of 20 °C, 35 °C and 50 °C. As to CPBs, Fall et al. (2010) have conducted laboratory tests on different types of CPB specimens at the curing temperatures of 2 °C, 20 °C, 35 °C and 50 °C, for investigating the compressive and split tensile strength, modulus of elasticity, stress–strain behavior of these CPBs. Fall and Samb (2009) have evaluated the strength of CPB specimens at different high temperatures (100, 200, 400 and 600 °C). Furthermore, Fall and Pokharel (2010) have carried out an experiment to study the combined effect of temperature and sulphate on the strength development of CPBs that are cured at different temperatures of 2 °C, 20 °C, 35 °C and 50 °C. Although former researchers have made contributions to understanding the influence of curing temperature on the mechanical performance of concrete and CPB, corresponding studies are still very limited. Besides, although CGFB, concrete and CPB are all cemented materials, they are still different from each other in some aspects such as aggregate used, mix proportion and operating conditions. Hence, the results obtained from the studies of concrete and CPB are not suitable for CGFB. There is an urgent need to understand the effect of curing temperature on the mechanical properties of CGFB materials.

Aa a non-destructive testing (NDT) method, acoustic emission (AE) monitoring has been widely and intensively used in the field of civil engineering for structural health monitoring (e.g., Shiotani et al. 2001; Shiotani 2006; Carpinteri et al. 2011; Prem and Murthy 2016.). The advantages of AE technique are that the position of the developing cracks can be determined and also the entire structure can be tested without interrupting the performance of the structure (Behnia et al. 2014). In the past few years, researchers have used AE monitoring technique to study the mechanical performance of concrete. AE parameters such as accumulated hits, signal strength and energy are successfully used to identify and characterize the process of concrete failure (e.g., Ohtsu and Tomoda 2007). For instance, Ohtsu et al. (2002) have used AE technique to assess the damage state of reinforced concrete (RC) beams under incremental cyclic loading. Colombo et al. (2003) have used AE technique to study the fracture process in RC beams. Nair and Cai (2010) have evaluated the damage conditions of concrete bridges based on AE signals. Some other researchers have also extended the application of AE monitoring technique to concrete structures (e.g., Benavent-Climent et al. 2012; Abadelrahman et al. 2014; Sagasta et al. 2016). Based on the wide and extensive utilization of AE technique in the field of concrete, several attempts have been made to study the mechanical behavior of CPB using AE monitoring technique. Liu et al. (2013) have used the AE technique to obtain the stress–strain behavior of CPB specimens with different mix proportions under uniaxial compression. Gong et al. (2014) have examined the b-value features of the AE signals obtained from loading and unloading tests of CPB samples. However, the application of AE technique to CPBs is still very limited. To date, no studies have been reported on the usage of AE technique in CGFB materials. This encourages the present authors to initiate the corresponding research.

The environment temperature around CPB structures can be affected by the factors as listed as follows (e.g., Rawlings and Phillips 2001; Fall et al. 2009; Fall and Pokharel 2010): (1) the depth of the mine and geological conditions (the temperature increases with the depth due to geothermic gradient), (2) the geographical condition of the mine (e.g., permafrost region), (3) other human-induced thermal factors such as ventilation.

In consideration of the facts that are mentioned above, the current study will be carried out to investigate the effect of curing temperature on the

UCS development of CGFB with the help of AE and infrared thermography techniques. This paper is organized as follows: (1) The experimental program, i.e., the materials used, the preparation of CGFB specimens and the tests done are presented in Sect. 2; (2) The obtained results and corresponding discussions are demonstrated in Sect. 3; (3) The conclusions are presented in the final section.

2 Experimental Program

2.1 Materials

Coal gangue, fly ash, cement and water are mixed to prepare the CGFB specimens. The coal gangue used is obtained from a coal mine in Hebei province of China, the fly ash used is from a power plant near this coal mine, the cement used is ordinary Portland cement 425# that is bought from the market, and the water used is tap water. Table 1 exhibits the main chemical compositions of the cement used, and Table 2 shows the chemical properties of the coal gangue and fly ash used.

2.2 Preparation of the CGFB Specimens

According to the mix proportion shown in Table 3, a total number of 108 CGFB samples are prepared: the CGFBs are cured at 4 kinds of temperatures (20 °C, 50 °C, 75 °C, and 90 °C) for 3 kinds of periods (1, 3 and 7 days) and tested by 3 kinds of experimental programs (measurement of elasticity modulus, UCS tests coupled with AE monitoring and thermal infrared observation), with each testing program conducted in triplicate. The required amount of coal gangue, fly ash, cement and water are blended and homogenized in a mortar mixer until obtaining the desired CGFB mixtures. It is noted that the mix proportion for all the CGFB samples is the same, as shown in Table 3. Afterwards, the produced CGFBs are poured into curing moulds with the dimension of 10 cm × 10 cm × 10 cm and 30 cm × 15 cm × 15 cm in length × width × height to form specimens for UCS tests (coupled with AE monitoring and thermal infrared observation)) and measurements of elasticity modulus, respectively. These CGFB specimens are then cured in a standard curing chamber (type: HS-225) at different curing temperatures and for various curing time.

Table 1 Main chemical compositions of the cement used

Chemical compositions (mass%)						
	SiO_2	Al_2O_3	Fe_2O_3	CaO	MgO	SO_3
Cement	19.31	4.93	3.12	63.15	3.26	2.32

2.3 Testing Methods

Since the CGFB specimens are cured at 4 kinds of temperatures (20, 50, 75 and 90 °C) for 3 kinds of periods (1, 3 and 7 days), there are a total number of 12 curing processes. When each curing process of the CGFB specimens are completed with the required age and temperature, two sets of CGFB specimens are taken out from the curing chamber. One set includes 6 CGFB specimens, of which 3 are used for the measurement of axial compressive strength, and the average values are used, while the other 3 are tested to obtain parameters for the calculation of elasticity modulus, as presented in Eq. (2). The following equation is used to calculate the axial compressive strength (GB/T50081-2002 2003):

$$f_{cp} = \frac{F}{A} \tag{1}$$

where f_{cp} is the axial compressive strength of the CGFB sample, F is the axial load on the CGFB when it fails, A is the loaded area (15 × 15 cm^2 in this study). As mentioned above, the average value of f_{cp} is used to calculate the elasticity modulus (GB/T50081-2002 2003):

$$E_c = \frac{F_a - F_0}{A} \cdot \frac{L}{\varepsilon_a - \varepsilon_0} \tag{2}$$

where E_c is the elasticity modulus, F_a is the axial load on the CGFB when the stress reaches a third of the axial compressive strength (f_{cp}), F_0 is the axial load when the stress increases to 0.5 MPa, L is the gauge length (15 cm in this study), ε_a and ε_0 are the average values of axial deformation in the CGFB corresponding to the load of F_a and F_0, respectively.

ε_a and ε_0 can be obtained as follows (GB/T50081-2002 2003):

As shown in Fig. 1, the load F_0 is applied on the CGFB specimen and kept constant for 60 s. In the

Table 2 Chemical properties of the coal gangue and fly ash used

Chemical compositions (mass%)							
	SiO_2	Al_2O_3	Fe_2O_3	CaO	K_2O	TiO_2	S
Coal gangue	47.75	19.59	10.23	14.74	0.97	1.85	4.87
Fly ash	52.63	23.67	12.78	5.31	1.74	2.45	1.42

Table 3 Mix proportion of the CGFB specimens

Solids content/wt.%	Coal gangue content/wt.%	Fly ash content/wt.%	Cement content/wt.%
80.0	50.0	20.0	10.0

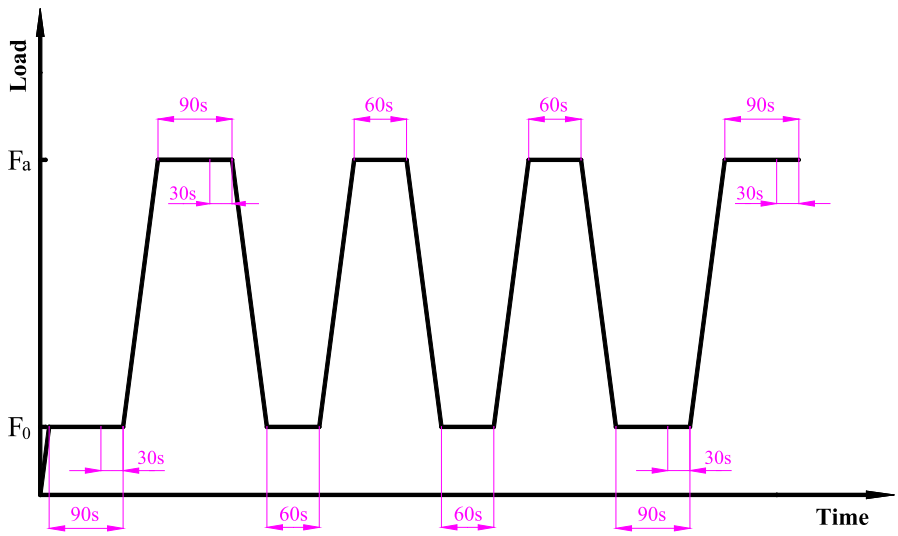

Fig. 1 Loading process on the CGFB

following 30 s, the average deformation ε_0 of the CGFB is measured by the elastic modulus measuring instrument (type: TM-II, as shown in Fig. 2). The load is remained unchanged for 60 s when it reaches to F_a. Similarly, ε_a is also obtained in the following 30 s. In the next stage, the load shown in Fig. 1 is applied on the CGFB but ε_0 and ε_a are only recorded in '30 s' stages when the load respectively reaches to F_0 and F_a. As a result, ε_0 and ε_a can be obtained for calculating the elasticity modulus according to Eq. (2).

The other set of the CGFB samples are subjected to the UCS tests also in triple. The rock mechanics testing apparatus (type: TAW-2000), which has the maximum load of 2000 kN and can display the stress–strain relation in real time, is used for the UCS tests. During the process of UCS testing, the CGFB sample is subjected to AE monitoring and thermal infrared observation simultaneously. PCI-2 AE Monitor System is used to record and display the characteristic parameters of the AE signals. An infrared thermography is used to record the average infrared radiation temperature (AIRT) evolution of the CGFB specimen during the UCS test. The camera used is Fluke Ti400 with the temperature range between − 20 and 1200 °C, resolution of 320 × 240 pixel, and sensitivity of 0.05 °C. Figure 3 shows the UCS test on a cubic CGFB sample coupled with AE monitoring and thermal infrared observation in the current study. Before the test, two thin films of Vaseline are coated on the end surfaces of the two AE sensors, respectively, in order to ensure favorable contact of the sensors with the CGFB sample. A rubber band is used to fix the two AE sensors and made them contact with the CGFB sample all the time during the test.

During the procedure of testing and monitoring, the compressive loading rate is kept at 0.2 mm/min, the

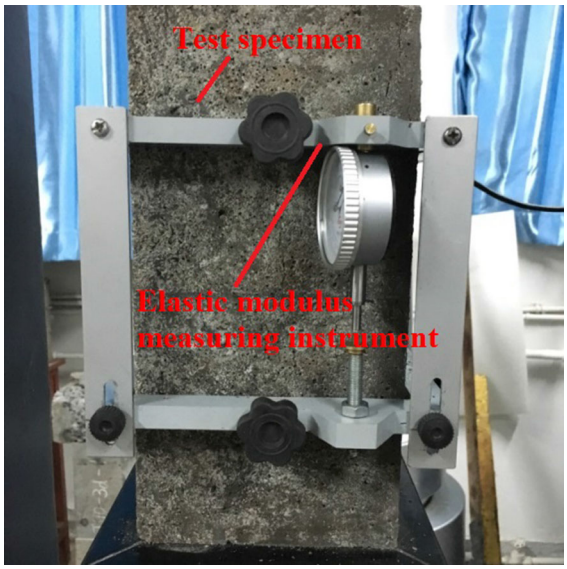

Fig. 2 Measurement of elasticity modulus

monitoring sampling rate of AE signals is set as 1 MSPS (i.e., million samples per second), and the gain for preamplifier is 40 dB. In order to minimize the interference of noise, the threshold value is set at 55 dB.

3 Results and Discussion

3.1 UCS and Elastic Modulus

Figure 4 illustrates the stress–strain curve of each CGFB sample obtained from UCS tests.

In order to reveal the effect of curing temperature (20 °C, 50 °C, 75 °C and 90 °C are selected) on the development of UCS in CGFB, the average UCS values for the CGFB specimens are obtained based on Fig. 4 and showed in Fig. 5. As expected, the UCS of CGFB increases with the curing time. From this figure, it can also be found that a higher curing temperature leads to a higher UCS in the CGFB structure. Especially in the very early age (0–3 days), the UCS of CGFB significantly increases with the curing temperature. This is because during this curing period, the effect of a higher curing temperature is highly remarkable to accelerate the binder hydration progress, which generates a large amount of hydration products to increase the UCS of CGFB. From the 3 to 7th day, the binder hydration rate decreases, thus the development of UCS in the CGFB also slows down.

Figure 5 also shows that, when the curing temperature increases from 20 to 50 °C and then to 75 °C, the UCS of CGFB increases dramatically. When the curing temperature increases from 75 to 90 °C, the UCS values of the CGFB specimens cured for 1 day and 3 days increase slowly, but the UCS of CGFB cured for 7 days decreases. This is due to the fact that, when the curing temperature increases in an appropriate range, it can exert a positive influence on the UCS development by promoting the binder hydration course. However, if the curing temperature is too high, it would exert a negative effect on the UCS development in CGFB, by generating excessive thermal stress on the CGFB and thus destroying its structure. From 0 to 3rd day, the binder hydration progress is strong and very sensitive to the curing temperature. Raising the curing temperature during this period can effectively speed up the binder hydration rate and thus contribute to the UCS development. Thereafter (3–7 days) the binder hydration process slows down and the effect of curing temperature on it weakens. The positive contribution of increasing the curing temperature to the UCS development is not able to conquer the UCS reduction induced by the negative effect of a too high

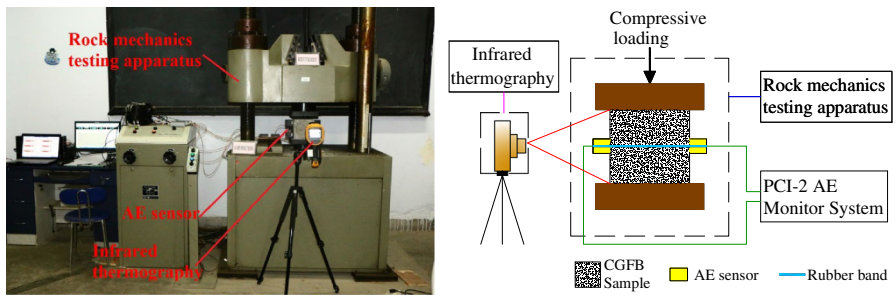

(a) Real photo **(b)** Schematic diagram

Fig. 3 UCS test coupled with AE monitoring and thermal infrared observation

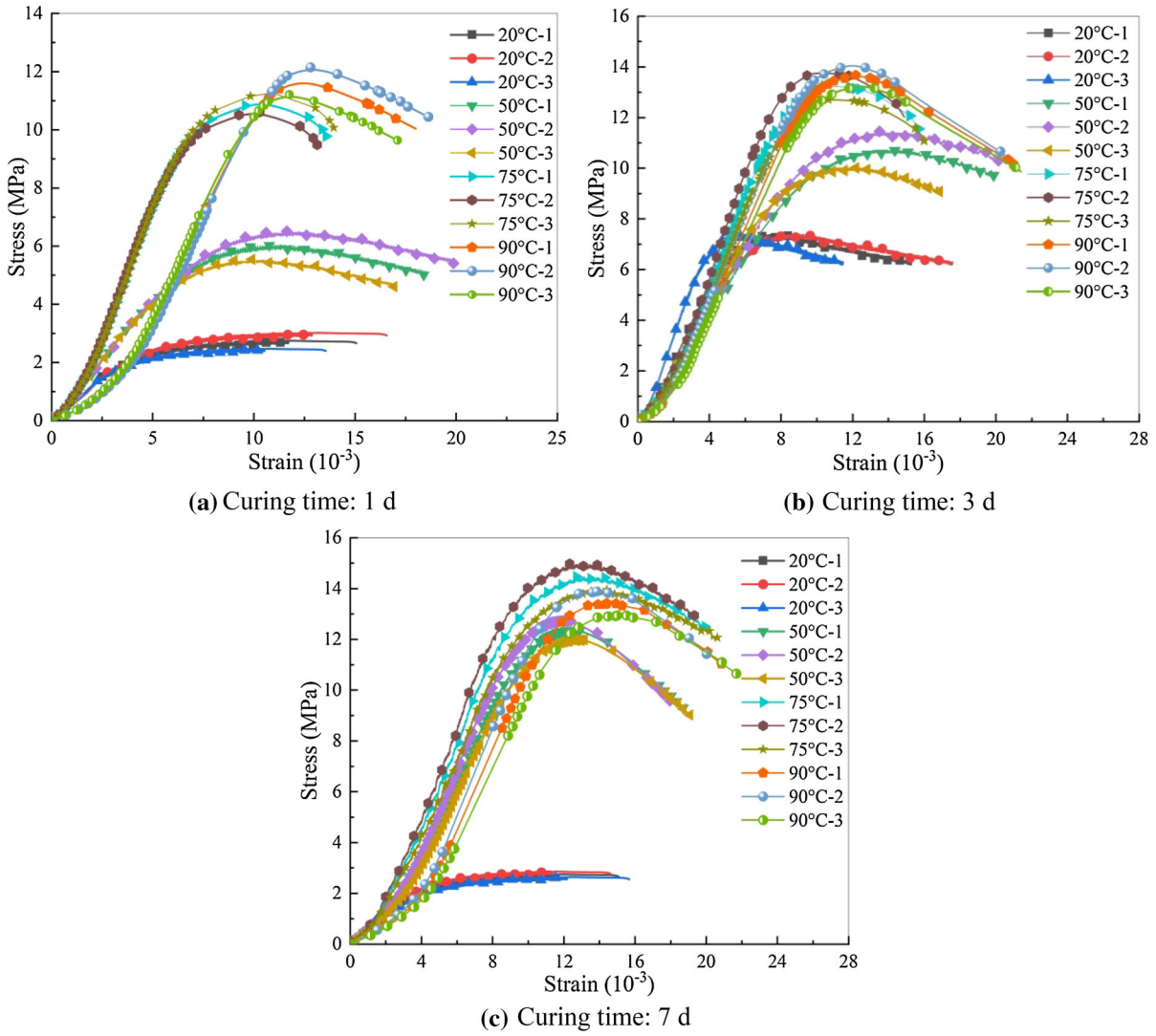

Fig. 4 Stress–strain curve for each CGFB specimen obtained from UCS tests

curing temperature. It can be expected that there must exist a certain threshold for the curing temperature, and if the curing temperature exceeds the threshold, the UCS of CGFB would decrease.

Table 4 lists the test results of elastic modulus for all the CGFB specimens. It is pointed out that the specimen number in Table 4, for instance, T20-1d-1 represents the CGFB sample 1 cured at the temperature of 20 °C for 1 day. Figure 6 illustrates the influence of curing temperature on the elastic modulus of the CGFB specimens. As expected, the elastic modulus of CGFB develops with the curing time. Similar results (with Fig. 5) can be noticed in Fig. 6 that, a higher curing temperature is associated with a higher value of elastic modulus of the CGFB specimen, except that a too high curing temperature (90 °C) exerts a negative effect on the elastic modulus.

3.2 Stress Evolution and Cumulative Count of AE

Taking the CGFB specimens cured for 7 days as examples, Fig. 7 displays the effect of curing temperature on the stress evolution of the CGFB structures versus time and the cumulative count of AE during the UCS tests. All these figures (Figs. 7a–d) illustrate almost the same results of regularity: the cumulative

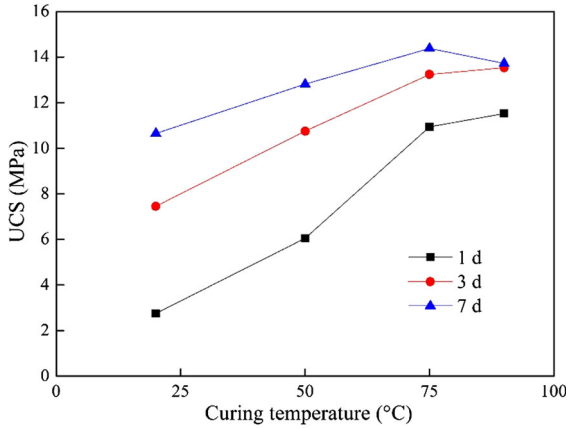

Fig. 5 Effect of curing temperature on the evolution of UCS of CGFB versus curing time

counts of AE achieve the maximum number when the stress reaches its peak value.

The whole stress evolutionary process versus time in the CGFB under UCS testing can be divided into 5 stages (Fig. 8): (1) initial compaction stage (o–a); (2) linear elastic stage (a–b); (3) elastoplastic stage (b–c); (4) plastic stage (c–d); (5) failure stage (d–e). Due to the uniaxial compression induced closure of the pores and micro cracks in the CGFB specimen, almost no AE events occur during the initial stage of loading. In the linear elastic stage, since few cracks are generated inside the CGFB structure, very few AE signals can be recorded. When it comes to the elastoplastic stage, the volumetric strain of the CGFB structure changes from compression to expansion before failure and the AE counts begin to increase with the increase of stress. Afterwards, with the continuous increase of the stress and when it reaches to the maximum, the continuous generation of new fracture and extension of old cracks result in the failure of the CGFB structure, and meanwhile, the cumulative counts of AE also reach the peak at the end of the plastic stage. And then during the failure stage, the CGFB sample still has bearing capacity to a certain extent, hence a definite number of AE events can be recorded. After that, the cumulative counts of AE gradually decrease to zero.

It can also be noticed from Fig. 8 that, the higher the peak stress (i.e., UCS) of the CGFB is, the more the maximum cumulative counts of AE are. This is because more energy is released during the uniaxial compressive deformation and damage of a CGFB structure with a higher value of stress, consequently more AE events occur during this process. Corresponding results have been illustrated in Fig. 5 that, with the increase of curing temperature from 20 to 50 °C and then to 75 °C, the peak stress in the CGFB sample increases, and the AE cumulative counts recorded also increase. In an appropriate range of temperature, raising the curing temperature can notably contribute to the acceleration of binder hydration process and thus the increase of stress. However, when the curing temperature increases to 90 °C that is beyond the appropriate range, the overly high temperature exerts a negative influence on the CGFB structure and thus reduces its peak stress and the AE cumulative counts. The obtained outcomes demonstrate that there is a strong relevance among the curing temperature, stress development in the CGFB, and the AE signal.

The mutation of AE cumulative counts is a sign of the failure of CGFB samples. The results shown in Fig. 8 indicate that the CGFB structures have different AE features at different loading stages. Therefore, the evolution of AE signals can be used to predict if the CGFB structures are stable under compressive load and when they are damaged by destabilization.

3.3 Evolution of Cumulative Mechanical Energy, Cumulative AE Energy and AIRT

When the CGFB sample is subjected to the UCS test, as the strain increases with the external loading, the mechanical energy of the loading system is transformed into strain energy. With the increase of strain, the crack initiation, propagation, coalescence and interaction can finally lead to the failure of the CGFB structure. In the meantime, plenty of AE events are generated during the failure process, and some of the strain energy turn into AE energy. On the other hand, due to the friction between particles within the CGFB specimen, some of the strain energy is dissipated in the form of thermal energy, which causes temperature increase in the specimen.

The mechanical energy that is provided by the loading system can be calculated by the following equation:

$$W = \int_0^x F(t) \cdot dx \tag{3}$$

Table 4 Test results of elasticity modulus of the CGFB specimens

Specimen number	F_0/N	F_a/N	Axial compressive strength/MPa	ε_a–ε_0/mm	Elasticity modulus (average values)/GPa
T20-1d-1	11250	19575	2.61	0.070	0.881
T20-1d-2				0.061	
T20-1d-3				0.062	
T20-3d-1	11250	58500	7.8	0.243	1.211
T20-3d-2				0.292	
T20-3d-3				0.251	
T20-7d-1	11250	85500	11.4	0.310	1.538
T20-7d-2				0.325	
T20-7d-3				0.331	
T50-1d-1	11250	45225	6.03	0.186	1.116
T50-1d-2				0.205	
T50-1d-3				0.220	
T50-3d-1	11250	78750	10.5	0.294	1.499
T50-3d-2				0.303	
T50-3d-3				0.303	
T50-7d-1	11250	99225	13.23	0.326	1.779
T50-7d-2				0.331	
T50-7d-3				0.332	
T75-1d-1	11250	81225	10.83	0.314	1.419
T75-1d-2				0.341	
T75-1d-3				0.333	
T75-3d-1	11250	103950	13.86	0.369	1.651
T75-3d-2				0.373	
T75-3d-3				0.381	
T75-7d-1	11250	108450	14.46	0.346	1.833
T75-7d-2				0.357	
T75-7d-3				0.358	
T90-1d-1	11250	85500	11.4	0.309	1.655
T90-1d-2				0.293	
T90-1d-3				0.296	
T90-3d-1	11250	105750	14.1	0.380	1.703
T90-3d-2				0.365	
T90-3d-3				0.365	
T90-7d-1	11250	108000	14.4	0.379	1.714
T90-7d-2				0.389	
T90-7d-3				0.362	

where W is the mechanical energy, $F(t)$ denotes the compressive stress, x denotes the displacement, and t is the time.

The AE energy can be obtained by the following equation (Jiang et al. 2016):

$$E = \int_{t1}^{t2} \frac{1}{R}[U(t)]^2 \cdot dt \tag{4}$$

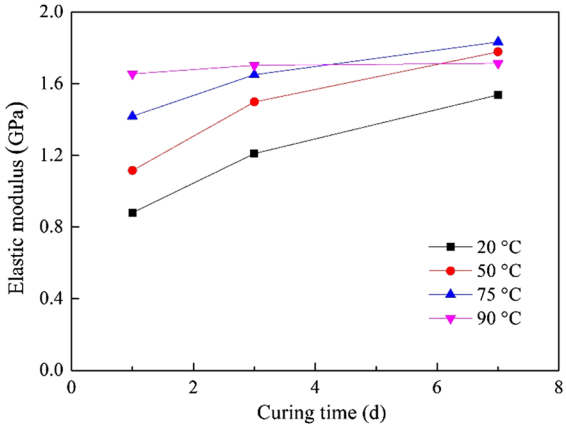

Fig. 6 Effect of curing temperature on elastic modulus of CGFB versus curing time

where E is the AE energy; $U(t)$ is the transient voltage, which is measured and recorded by the AE monitoring system; $t1$ and $t2$ are the starting and ending moments for the voltage transient measurement; and R denotes the internal resistance for the measuring circuit.

In order to understand the relationship between the mechanical, thermal and acoustic properties of the CGFB, different specimens cured for 7 days at various curing temperatures (20, 50, 75 and 90 °C) were subjected to the UCS test coupled with AE monitoring and thermal infrared observation, and the evolutions of the cumulative mechanical energy, cumulative AE energy and AIRT were measured and calculated, respectively, as shown in Fig. 9. It should be noted

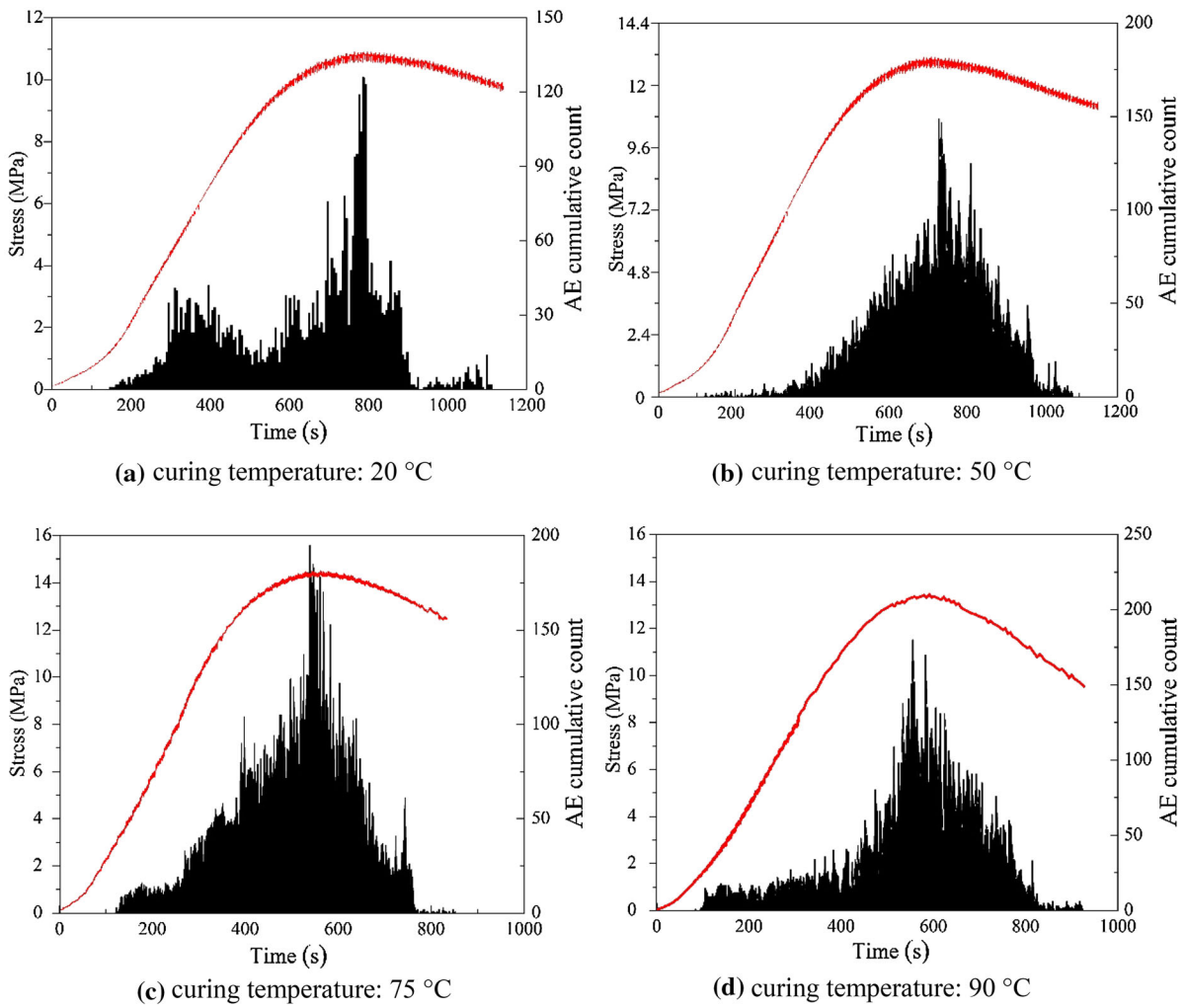

Fig. 7 Effect of curing temperature on stress evolution and cumulative count of AE in CGFB cured for 7 days

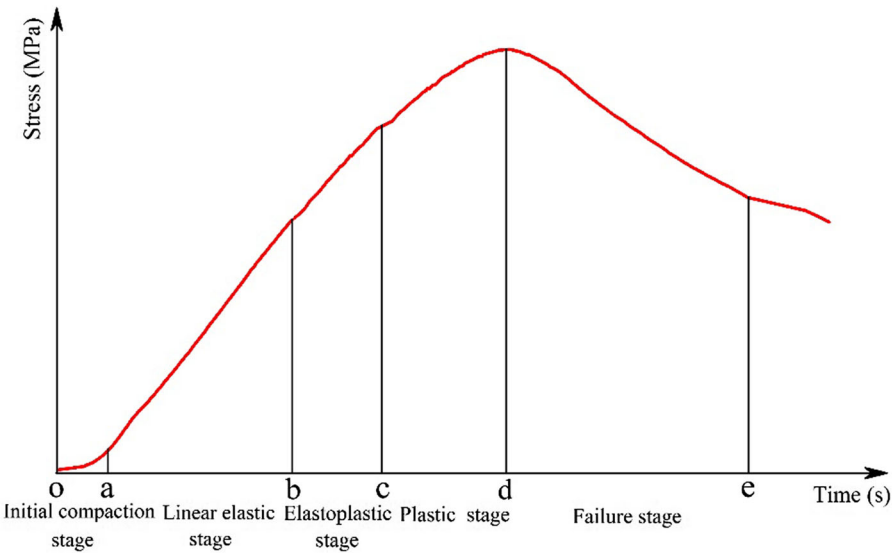

Fig. 8 Development of stress in the CGFB structure versus time during UCS testing

that, the CGFB samples cured at various temperatures were taken out from the curing chamber and placed for some time, ensuring that the initial temperatures for all the CGFB specimens tested are close to room temperature (about 20 °C).

From Fig. 9 it can be noticed that, with the elapse of the loading time, the change of the cumulative mechanical energy can be approximately divided into three stages, which are slow growth stage, transitional stage and linear growth stage. Similarly, the varying process of the cumulative AE absolute energy almost includes linear growth stage, rapid growth stage, and steady maintaining stage. During the test, the change of the AIRT can be approximately divided into four stages: OA, AB, BC and CD as seen in Fig. 9, and they stand for slow growth stage, steady growth stage, rapid growth stage and sharp decline stage, respectively. In the OA stage, the AIRTs of the CGFB specimens basically maintain at room temperature. This is due to the fact that in this stage, the microcracks within the CGFB are compacted and the generation of heat by friction is insignificant. Therefore, only a small part of the strain energy is converted into the thermal energy. Correspondingly, during the OA stage, the developments for the cumulative mechanical energy and cumulative AE absolute energy are respectively at the stages of slow growth and linear growth. With the continuous increase of the compressive load in the AB stage, the AIRT of the CGFB sample also increases rapidly and shows a linear trend. This is ascribed to the fact that the thermal energy generated by friction increases steadily with the linear increase of the compressive stress when the CGFB structure performs elastic behavior. It is known as the thermoelastic effect which refers to that, the rate of change in the temperature of a structure being loaded is directly related to the rate of change of the principal stress (Horstemeyer and Bammann 2010).

In the BC stage, with the steady increase of AIRT, the cumulative mechanical energy and cumulative AE absolute energy increase sharply in linear trends. Almost at the end of the BC stage (or the start of the CD stage), the AIRT of the CGFB specimen reaches the maximum value, and almost at the same time, the cumulative AE absolute energy also reaches the peak value. It can be forecasted that at this moment, the UCS of the CGFB also approaches to the peak value. When it comes to the CD stage, the AIRT of the CGFB begins to decrease. This is because of the failure of the CGFB structure, so a great deal of the strain energy is converted to the AE energy but the friction induced temperature increase in the CGFB becomes insignificant. Besides, a part of the thermal energy dissipates into the surrounding environment, which results in a decrease in the AIRT of the CGFB.

Based on the above discussions, it can be concluded that the failure of a CGFB structure can be characterized by combining the thermal infrared observation and AE monitoring for pre-warning in practice.

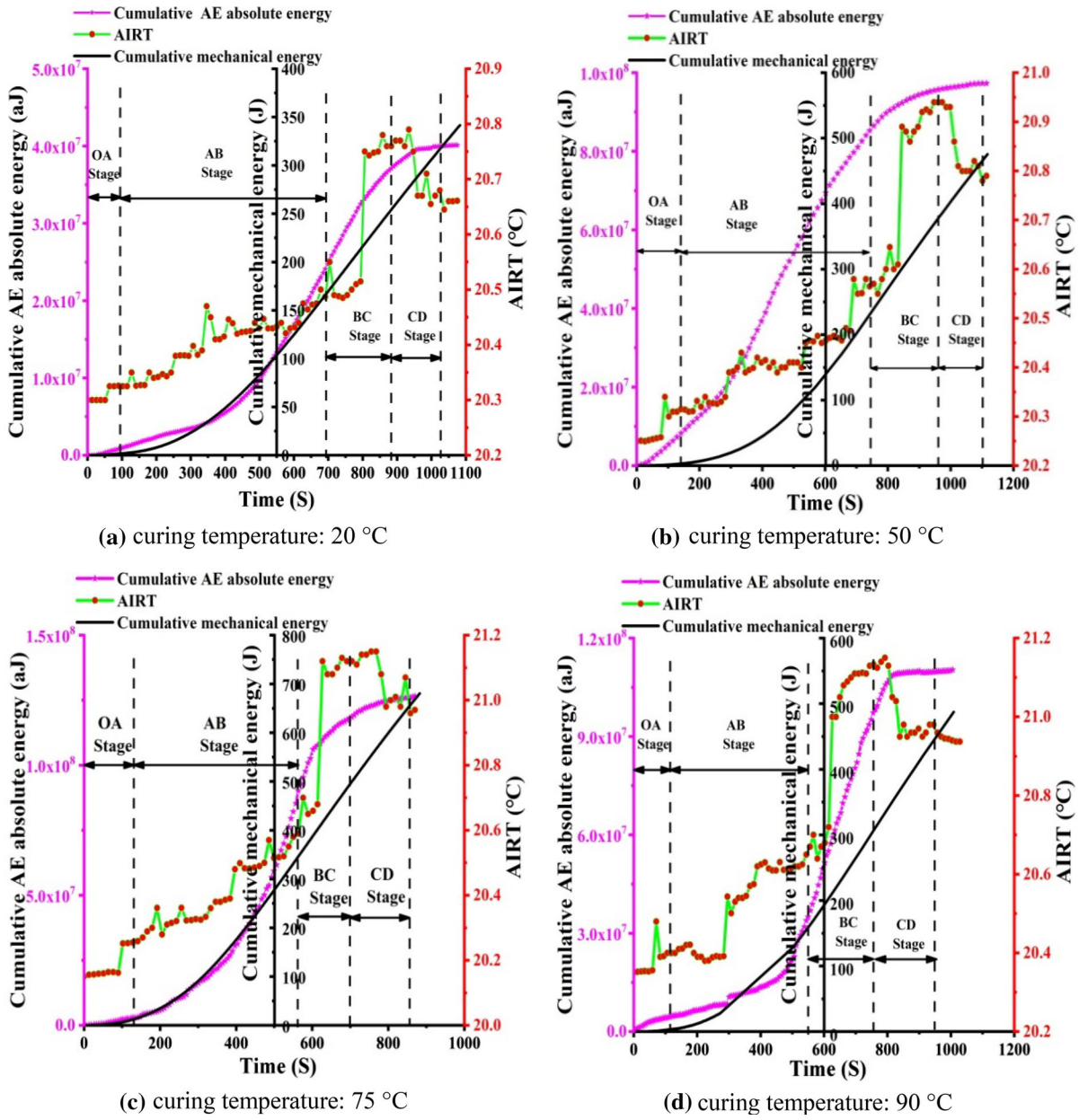

Fig. 9 Evolutions of the cumulative mechanical energy, cumulative AE energy and AIRT for the CGFB specimens cured for 7 days at different curing temperatures

From Fig. 9, it can also be found that the effect of curing temperature on the cumulative mechanical energy, AIRT and cumulative AE absolute energy, as demonstrated in Table 5.

From Table 5 it can be clearly noticed that, when the curing temperature increases from 20 to 50 °C and then to 75 °C, all the increment in the cumulative mechanical energy, AIRT and cumulative AE absolute energy of the CGFBs increase. This is due to the fact that a higher curing temperature can accelerate the process of binder hydration, and thus generate more hydration products to improve the CGFB strength. Apparently, it needs more mechanical energy to destroy a CGFB structure with a higher strength. Meanwhile, more mechanical energy is converted to the thermal and acoustic energy. Therefore, a higher

Table 5 The increment in the cumulative mechanical energy, AIRT and cumulative AE absolute energy of the CGFBs (cured for 7 days with different curing temperatures) from 0 to 850 s

Curing temperature/°C	Cumulative mechanical energy/J	AIRT/°C	Cumulative AE absolute energy/aJ
20	232.34	0.45	3.57×10^7
50	291.45	0.65	9.23×10^7
75	648.32	0.90	12.61×10^7
90	365.47	0.60	10.94×10^7

curing temperature (in an appropriate range) is associated with higher increment in the cumulative mechanical energy, AIRT and cumulative AE absolute energy. However, it is also discovered that when the curing temperature increases from 75 to 90 °C, all the increment in the cumulative mechanical energy, AIRT and cumulative AE absolute energy of the CGFBs decrease. The reason has been discussed earlier that, if the curing temperature is too high (exceeding a critical value), it can exert a negative effect on the CGFB strength and thus damage the structure. It is obvious that less mechanical energy is required to destroy a damaged structure than a healthy one.

4 Conclusions

This study experimentally investigates the mechanical behavior and AE characteristics of CGFB under various curing temperatures. On the basis of the obtained results in this study, the following conclusions can be drawn.

1. In an appropriate temperature range, increasing the curing temperature can signally accelerate the binder hydration rate, contributing to higher elastic modulus and strength development in CGFB. But when the curing temperature is overly high (exceeding a threshold value), it will exert a negative effect on the mechanical performance of a hardened CGFB structure.
2. The thermal factors exert a significant influence on the AE properties of hardened CGFB. In a suitable range of temperature, a higher curing temperature is associated with more AE cumulative counts and energy recorded. However, if the curing temperature is beyond the proper range, it will decrease the recorded AE cumulative counts and energy.
3. Similarly, increasing the curing temperature in an appropriate range can effectively result in the increment in the cumulative mechanical energy, AIRT and cumulative AE absolute energy of a hardened CGFB structure. The cumulative mechanical energy, AIRT and cumulative AE absolute energy increase roughly following the development of stress in the CGFB structure versus time. From the viewpoint of energy, this process from deformation to failure and then to collapse of the CGFB structure is a course of energy transformation.

Acknowledgements The authors would like to acknowledge the support from China Scholarship Council; Yue Qi Young Scholar Project, China University of Mining and Technology, Beijing; the State Key Laboratory for Coal Resources and Safe Mining, China University of Mining and Technology (Grant No. SKLCRSM16KFC04); and the guidance from the researchers of Beijing Key Laboratory for Precise Mining of Intergrown Energy and Resources.

References

Abadelrahman M, Elbatanouny MK, Ziehl PH (2014) Acoustic emission based damage assessment method for prestressed concrete structures: modified index of damage. Eng Struct 60:258–264

Behnia A, Chai HK, Shiotani T (2014) Advanced structural health monitoring of concrete structures with the aid of acoustic emission. Constr Build Mater 65:282–302

Benavent-Climent A, Gallego A, Vico JM (2012) An acoustic emission energy index for damage evaluation of reinforced concrete slabs under seismic loads. Struct Health Monit Int J 11:69–81

Carpinteri A, Lacidogna G, Niccolini G (2011) Damage analysis of reinforced concrete building by the acoustic emission technique. Struct Control Health Monit 18:660–673

Colombo S, Main IG, Forde MC (2003) Assessing damage of reinforced concrete beam using b-value analysis of acoustic emission signals. J Mater Civ Eng 15(3):280–286

Fall M, Pokharel M (2010) Coupled effects of sulphate and temperature on the strength development of cemented tailings backfills: portland cement-paste backfill. Cem Concr Compos 32:819–828

Fall M, Samb SS (2009) Effect of high temperature on strength and microstructural properties of cemented paste backfill. Fire Saf J 44(4):642–651

Fall M, Adrien D, Célestin JC, Pokharel M, Touré M (2009) Saturated hydraulic conductivity of cemented paste backfill. Miner Eng 22(15):1307–1317

Fall M, Célestin JC, Pokharel M, Touré M (2010) A contribution to understanding the effects of curing temperature on the mechanical properties of mine cemented tailings backfill. Eng Geol 114(3–4):397–413

GB/T50081-2002 (2003) Standard for test method of mechanical properties on ordinary concrete. China Architecture and Building Press, Beijing **(in Chinese)**

Gong C, Li C, Zhao K (2014) Experimental study on b-value characteristics of acoustic emission of cemented filling body under loading and unloading test. J Min Saf Eng 31(5):788–794 **(in Chinese)**

Horstemeyer MF, Bammann DJ (2010) Historical review of internal state variable theory for inelasticity. Int J Plast 26(9):1310–1334

Jiang D, Xie K, Jiang X, Chen J, Yuan X (2016) Statistical analysis of acoustic emission energy distribution during uniaxial compression of shale. Chin J Rock Mech Eng 35(s2):3822–3828 **(in Chinese)**

Liu X, Liu K, Zhao K, Hu J (2013) Strain rate effects and acoustic emission characteristics of tailing cement backfill under uniaxial compression. Electron J Geotech Eng 18:3919–3932

Nair A, Cai CS (2010) Acoustic emission monitoring of bridges: review and case studies. Eng Struct 32(6):1704–1714

Ohtsu M, Tomoda Y (2007) Acoustic emission techniques for rebar corrosion in reinforced concrete. Adv Constr Mater 41(3):615–621

Ohtsu M, Uchida M, Okamoto T, Yuyama S (2002) Damage assessment of reinforced concrete beams qualified by acoustic emission. ACI Struct J 417:411–417

Orosz K, Hedlund H, Cwirzen A (2017) Effects of variable curing temperatures on autogenous deformation of blended cement concretes. Constr Build Mater 149:474–480

Prem PR, Murthy AR (2016) Acoustic emission and flexural behaviour of RC beams strengthened with UHPC overlay. Constr Build Mater 123:481–492

Rawlings CA, Phillips HR (2001) Reduction of mine heat loads. In: Proceedings of the 7th international mine ventilation congress, pp. 381–389

Sagasta FA, Benavent-Climent A, Roldán A, Gallego A (2016) Correlation of plastic strain energy and acoustic emission energy in reinforced concrete structures. Appl Sci 6:84

Shiotani T (2006) Evaluation of repair effect for deteriorated concrete piers of intake dam using AE activity. Adv Mater Res 13:175–180

Shiotani T, Ohtsu M, Ikeda K (2001) Detection and evaluation of AE waves due to rock deformation. Constr Build Mater 15:235–246

Wu D, Yang B, Liu Y (2015a) Pressure drop in loop pipe flow of fresh cemented coal gangue-fly ash slurry: experiment and simulation. Adv Powder Technol 26(3):920–927

Wu D, Yang B, Liu Y (2015b) Transportability and pressure drop of fresh cemented coal gangue-fly ash backfill (CGFB) slurry in pipe loop. Powder Technol 284:218–224

Wu D, Zhang Y, Liu Y (2016a) Mechanical performance and ultrasonic properties of cemented gangue backfill with admixture of fly ash. Ultrasonics 64:89–96

Wu D, Sun G, Liu Y (2016b) Modeling the thermo-hydro-chemical behavior of cemented coal gangue-fly ash backfill. Constr Build Mater 111:522–528

Wu D, Hou Y, Deng T, Chen Y, Zhao X (2017) Thermal, hydraulic and mechanical performances of cemented coal gangue-fly ash backfill. Int J Miner Process 162:12–18

Xu G, Tian Q, Miao J, Liu J (2017) Early-age hydration and mechanical properties of high volume slag and fly ash concrete at different curing temperatures. Constr Build Mater 149:367–377

Zhao Q, Liu X, Jiang J (2015) Effect of curing temperature on creep behavior of fly ash concrete. Constr Build Mater 96:326–333